AD-A039 893 STANFORD UNIV CALIF GUIDANCE AND CONTROL LAB F/G 8/5
STUDY TO DEVELOP GRADIOMETER COMPENSATION TECHNIQUES.(U)
DEC 76 D B DEBRA, E J PELKA F19628-76-C-0109
UNCLASSIFIED AFGL-TR-77-0038 NL

| OF |
AD
A039893

END

DATE
FILMED
6-77

AFGL-TR-77-0038

STUDY TO DEVELOP GRADIOMETER COMPENSATION TECHNIQUES

by

Daniel B. DeBra and Eugene J. Pelka

Stanford University
Guidance & Control Laboratory
Department of Aeronautics and Astronautics
Stanford, California 94305

FINAL REPORT

August 1975 to July 1976

December 1976

Approved for public release. Distribution Unlimited

Prepared For

U.S. AIR FORCE GEOPHYSICS LABORATORY
AIR FORCE SYSTEMS COMMAND
UNITED STATES AIR FORCE
BEDFORD, MASSACHUSETTS 01731

SECURITY CLASSIFICATION OF THIS PAGE (When Data Entered)

REPORT DOCUMENTATION PAGE

READ INSTRUCTIONS BEFORE COMPLETING FORM

1. REPORT NUMBER: AFGL-TR-77-0038	2. GOVT ACCESSION NO.
3. RECIPIENT'S CATALOG NUMBER	
4. TITLE (and Subtitle): STUDY TO DEVELOP GRADIOMETER COMPENSATION TECHNIQUES	5. TYPE OF REPORT & PERIOD COVERED: Final Aug 75 — Jul 76
	6. PERFORMING ORG. REPORT NUMBER
7. AUTHOR(s): Daniel B. DeBra; Eugene J. Pelka	8. CONTRACT OR GRANT NUMBER(s): F19628-76-C-0109
9. PERFORMING ORGANIZATION NAME AND ADDRESS: Stanford University, Guidance & Control Laboratory, Stanford, California 94305	10. PROGRAM ELEMENT, PROJECT, TASK AREA & WORK UNIT NUMBERS: 61102F; Work Unit No. 8607[illegible] 02
11. CONTROLLING OFFICE NAME AND ADDRESS: Air Force Geophysics Laboratory, Hanscom AFB, Mass 01731, Monitor/James Hammond/LWG	12. REPORT DATE: Dec 76; 13. NUMBER OF PAGES: 32 (72) 37p.
14. MONITORING AGENCY NAME & ADDRESS (if different from Controlling Office)	15. SECURITY CLASS. (of this report): Unclassified
	15a. DECLASSIFICATION/DOWNGRADING SCHEDULE

16. DISTRIBUTION STATEMENT (of this Report)

Approved for public release; distribution unlimited

DDC RECEIVED MAY 26 1977 C

17. DISTRIBUTION STATEMENT (of the abstract entered in Block 20, if different from Report)

18. SUPPLEMENTARY NOTES

407 256

19. KEY WORDS (Continue on reverse side if necessary and identify by block number)

gravity gradiometer; Rotating Hughes Gravity Gradiometer (RGG); Bell Aerospace, C.Stark Draper Lab., Eotvos Units, spin axes, sensors; stress relaxation, creep.

20. ABSTRACT (Continue on reverse side if necessary and identify by block number)

see other side

DD FORM 1 JAN 73 1473 EDITION OF 1 NOV 65 IS OBSOLETE
S/N 0102-LF-014-6601

SECURITY CLASSIFICATION OF THIS PAGE (When Data Entered)

There are three moving base gravity gradiometers currently under development. The instruments are being deveLed at the Hughes Research Labs ~~[Ref. 1]~~, the Bell Aerospace Corp. ~~[2]~~, and the Charles Stark Draper Lab. ~~[3, 4]~~. The design goal for each of the sensors is 1 Eötvös Unit (EU). The group includes sensors designed specifically to measure the gravity gradient, as well as sensors which utilize existing accelerometers to provide a gradient estimate. The Hughes and Bell instruments rotate, modulating the information. This rotation transfers the gravity gradient signal to a higher frequency, quieter, portion of the spectrum, and can separate the signal from some sources of instrument bias. The Draper Lab. sensor measures the gradient signal at zero frequency and uses a sophisticated flotation suspension system to isolate the sensing element from errors induced by rotation and jitter.

A system of at least three instruments of any one type is required in order to provide a complete gravity gradient tensor estimate. The primary objective of this paper is to define the optimal relative orientations of the three sensors which comprise a minimum gravity gradient measurement system. In addition, the effects of different relative sensor orientations when a fourth, redundant sensor is included, are considered.

FOREWORD

A portion of the work done under this contract has been combined into the Final Report of the previous contract in order to keep the material on model fitting as an integrated report. That report represents the principal parts of the doctoral thesis of E. J. Pelka. Some work that has been done since that thesis study is incorporated as Chapter I of this Final Report, which represents the last part of the studies done in this subject area under the current contract though not all of it.

The literature search on stress relaxation/creep reported in Chapter II was largely negative. Discussions with people in the Materials Science Department at Stanford and elsewhere indicate little is known about the mechanism and nature of microstrains. Professor John Shyne has recently spent several months in Japan interacting with a group doing research in this area. It is hoped that a better understanding of this phenomena will improve our ability to interpret long term variations in gradiometers which have been observed in some of the test data reported by the developers.

Research that was started in the evaluation of small accelerations to be used for the on-line correction of kinematically induced errors began with disappointing performance; thus it was felt it would be better omitted in this Final Report.

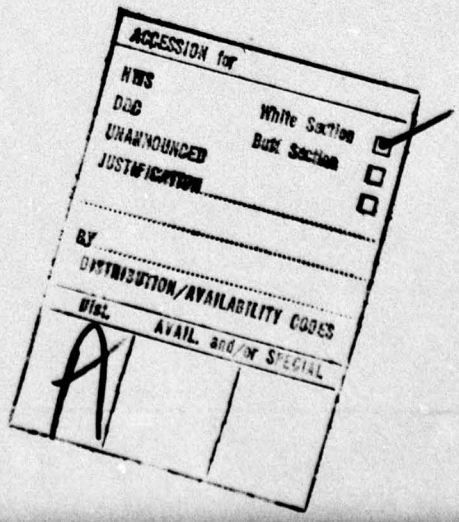

Chapter I

INTRODUCTION

There are three moving base gravity gradiometers currently under development. The instruments are being developed at Hughes Research Labs [Ref. 1], the Bell Aerospace Corp. [2], and the Charles Stark Draper Lab. [3, 4]. The design goal for each of the sensors is 1 Eötvös Unit (EU). The group includes sensors designed specifically to measure the gravity gradient, as well as sensors which utilize existing accelerometers to provide a gradient estimate. The Hughes and Bell instruments rotate, modulating the information. This rotation transfers the gravity gradient signal to a higher frequency, quieter, portion of the spectrum, and can separate the signal from some sources of instrument bias. The Draper Lab. sensor measures the gradient signal at zero frequency and uses a sophisticated flotation suspension system to isolate the sensing element from errors induced by rotation and jitter.

A system of at least three instruments of any one type is required in order to provide a complete gravity gradient tensor estimate. The primary objective of this paper is to define the optimal relative orientations of the three sensors which comprise a minimum gravity gradient measurement system. In addition, the effects of different relative sensor orientations when a fourth, redundant sensor is included, are considered.

A. THE GRAVITATIONAL FIELD AND ITS GRADIENT

A gravitational field is conservative and may be expressed as a scalar function φ of position $\vec{r}$ relative to the attracting body. The gravitational acceleration $\vec{g}$ due to the body, at any point $\vec{r}$, may be written as

$$\vec{g} = \nabla\varphi(\vec{r}) \ . \qquad (1)$$

Expressing $\vec{g}$ in a set of Cartesian coordinates, (1) may be rewritten as

$$[\vec{g}]^T = \begin{bmatrix} \frac{\partial \Phi}{\partial x} & \frac{\partial \Phi}{\partial y} & \frac{\partial \Phi}{\partial z} \end{bmatrix} . \qquad (2)$$

The spatial gradient of the gravity vector $\vec{g}$, written in Cartesian coordinates is the second order tensor

$$[\nabla \vec{g}] = \begin{bmatrix} \frac{\partial^2 \Phi}{\partial x^2} & \frac{\partial^2 \Phi}{\partial x \partial y} & \frac{\partial^2 \Phi}{\partial x \partial z} \\ \frac{\partial^2 \Phi}{\partial y \partial x} & \frac{\partial^2 \Phi}{\partial y^2} & \frac{\partial^2 \Phi}{\partial y \partial z} \\ \frac{\partial^2 \Phi}{\partial z \partial x} & \frac{\partial^2 \Phi}{\partial z \partial y} & \frac{\partial^2 \Phi}{\partial z^2} \end{bmatrix} . \qquad (3)$$

In order to determine completely the gravity gradient tensor of (3), all of the independent components must be measured. For a conservative gravitation force: [5]

$$\nabla \times \vec{g} = 0 ; \qquad (4)$$

and

$$\nabla \cdot \vec{g} = 0 . \qquad (5)$$

Equation (4) demonstrates the symmetry of the gradient tensor. Equation (5) is Laplace's equation and requires that the sum of the diagonal components of the gradient tensor is zero. Since the gradient tensor is symmetric, no more than six of its nine components are independent. The scalar Laplace equation (5) further reduces the total number of independent elements by one. Hence, only five of the nine elements of the gravity gradient tensor are independent. Complete determination of the gravity gradient tensor at any point requires only five measurements.

To follow convention, the gradient tensor will be represented by $\vec{\vec{\Gamma}}$,

$$\overleftrightarrow{[\Gamma]} \triangleq \begin{bmatrix} \Gamma_{xx} & \Gamma_{xy} & \Gamma_{xz} \\ \Gamma_{xy} & \Gamma_{yy} & \Gamma_{yz} \\ \Gamma_{xz} & \Gamma_{yz} & \Gamma_{zz} \end{bmatrix} \tag{6}$$

B. HUGHES' ROTATING GRAVITY GRADIOMETER

The rotating gravity gradiometer being developed at Hughes Research Labs measures gravity gradient at a nonzero frequency. The instrument, shown in Fig. 1, can be thought of as two identical arms connected by a flex pivot. The relative torque acting upon the arms is sensed by a piezoelectric transducer as the pivot is strained. The gravity gradient signal excites the instrument at its resonant frequency, which is twice the 17-5 Hz spin frequency.

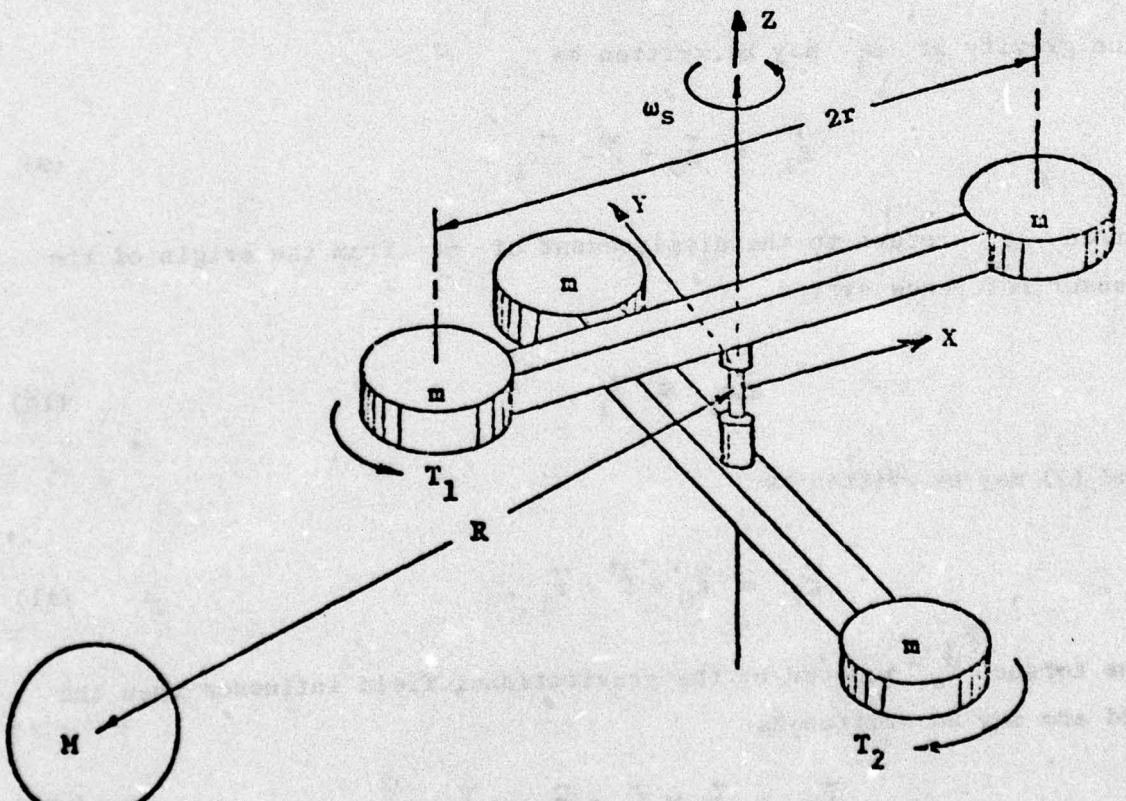

FIG. 1 HUGHES RESEARCH LABS ROTATING GRAVITY GRADIOMETER

B.1 Simplified Gradiometer Signal Development. Steady State Operation Approximation.

Consider the ideal dumbbell gradiometer oriented with its spin axis $\hat{z}_s$ horizontal as shown in Fig. 2. The vector $\vec{g}_0$ is the gravity vector at the origin of the sensor axis reference system and defines the local horizontal plane.

At any of the masses, m_1, for example, the gravity vector can be written in terms of $\vec{g}_0$ as in (7);

$$g_{1_j} = g_{0_j} + \frac{\partial g_j}{\partial k} \Delta k, \qquad \begin{matrix} j = x,y,z \\ k = x,y,z \end{matrix} \tag{7}$$

Using (6) and the definition

$$\vec{\Delta r} \triangleq (\Delta x, \ \Delta y, \ \Delta z)^T , \tag{8}$$

the gravity at m_1 may be written as

$$\vec{g}_1 = \vec{g}_0 + \vec{\vec{\Gamma}} \cdot \vec{\Delta r}_1 . \tag{9}$$

Since Δr_1 refers to the displacement of m_1 from the origin of the sensor reference system,

$$\vec{\Delta r}_1 \equiv \vec{r}_1 , \tag{10}$$

and (9) may be written as

$$\vec{g}_1 = \vec{g}_0 + \vec{\vec{\Gamma}} \cdot \vec{r}_1 . \tag{11}$$

The torque $\vec{T}_o$ induced by the gravitational field influence upon the odd arm may be written as

$$\vec{T}_o = \vec{r}_1 \times \vec{f}_1 + \vec{r}_3 \times \vec{f}_3 \tag{12}$$

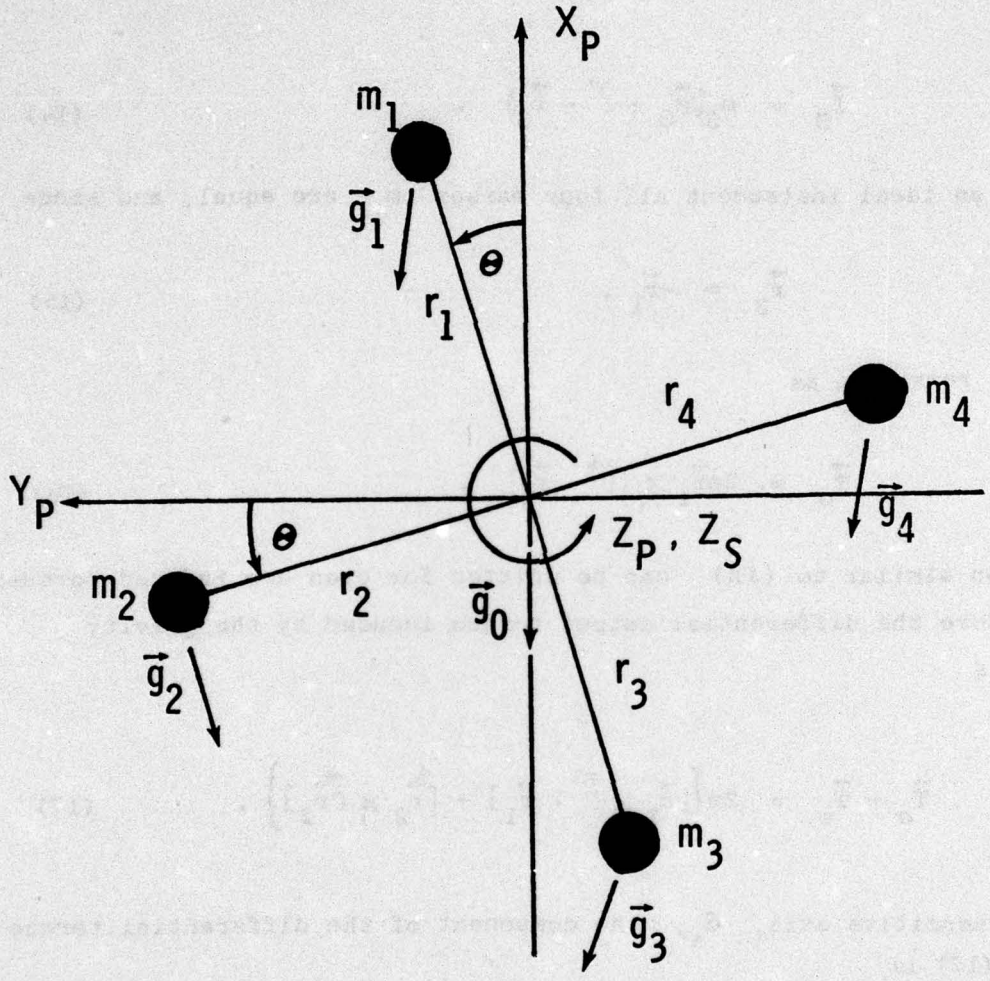
X_P
m_1
$\vec{g}_1$
θ
r_1
r_4
m_4
Y_P
θ
$\vec{g}_4$
Z_P , Z_S
m_2
r_2
$\vec{g}_0$
$\vec{g}_2$
r_3
m_3
$\vec{g}_3$

FIGURE 2

where

$$\vec{f}_1 = m_1\{\vec{g}_0 + \vec{\vec{\Gamma}} \cdot \vec{r}_1\} \tag{13}$$

and

$$\vec{f}_3 = m_3\{\vec{g}_0 + \vec{\vec{\Gamma}} \cdot \vec{r}_3\} \quad . \tag{14}$$

Since for an ideal instrument all four masses m_i are equal, and since

$$\vec{r}_3 = -\vec{r}_1 \, , \tag{15}$$

(12) can be rewritten as

$$\vec{T}_o = 2m\vec{r}_1 \times \{\vec{\vec{\Gamma}} \cdot \vec{r}_1\} \quad . \tag{16}$$

An equation similar to (16) can be written for even arm induced torques and therefore the differential output torque induced by the gravity gradient is

$$\vec{T}_o - \vec{T}_e = 2m\left\{[\vec{r}_1 \times \vec{\vec{\Gamma}} \cdot \vec{r}_1] - [\vec{r}_2 \times \vec{\vec{\Gamma}}\vec{r}_2]\right\} . \tag{17}$$

Along the sensitive axis, $\hat{z}_s$, the component of the differential torque vector of (17) is

$$(\vec{T}_o - \vec{T}_e) \cdot \hat{z}_s = 2mr^2\left\{2(\Gamma_{yy} - \Gamma_{xx})\sin\theta\cos\theta + 2\Gamma_{xy}(\cos^2\theta - \sin^2\theta)\right\} \tag{18}$$

or

$$(\vec{T}_o - \vec{T}_e) \cdot \hat{z}_s = 2mr^2\left\{(\Gamma_{yy}-\Gamma_{xx})\sin 2\theta + 2\Gamma_{xy}\cos 2\theta\right\}. \tag{19}$$

By separating the inphase (sin 2θ) and quadrature (cos 2θ) components of output Eq. (19), measurements containing three of the five independent terms of the gravity gradient tensor are available.

C. BELL AEROSPACE CORP. GRADIOMETER

The sensitive elements of the Bell Aerospace Corp.'s gravity gradiometer are four modified Bell Model VII pendulous accelerometers. The accelerometers are mounted symmetrically on a spin table with their sensitive axes in the tangential direction defined by $\hat{s}$, where

$$\hat{s} = \hat{\omega} \times \hat{r} \ . \tag{20}$$

The nominal spin table rate is 0.5 Hz. A conceptual diagram of the Bell instrument was shown in Fig. 3. The instrument senses gravity gradient in the X-Y plane according to the equation

$$[(a_1 + a_2) - (a_3 + a_4)] = 2d\{(\Gamma_{yy} - \Gamma_{xx}) \sin(2\omega t) + 2\Gamma_{xy} \cos(2\omega t)\} \ . \tag{21}$$

Modulation of the output signal yields an inphase measurement of the off-diagonal gravity gradient tensor component, Γ_{xy}, and a quadrature measurement of the difference between two of the diagonal terms, $\Gamma_{xx} - \Gamma_{yy}$.

Comparison of (19) and (21) shows that the output equations for both of the rotating gravity gradiometers are equivalent.

D. DRAPER LABS GRAVITY GRADIOMETER

The Draper Lab's instrument senses the gravity gradient signal at zero frequency, i.e., the instrument does not rotate. A conceptual drawing of the Draper Lab's spherical gradiometer is shown in Fig. 4.

The spherical gradiometer uses a spherical float having dense masses attached at two points which provide a dumbbell mass distribution as shown in the figure. External torques are sensed about each of the two perpendicular axes (i, j) which define a plane normal to the between-the-weights

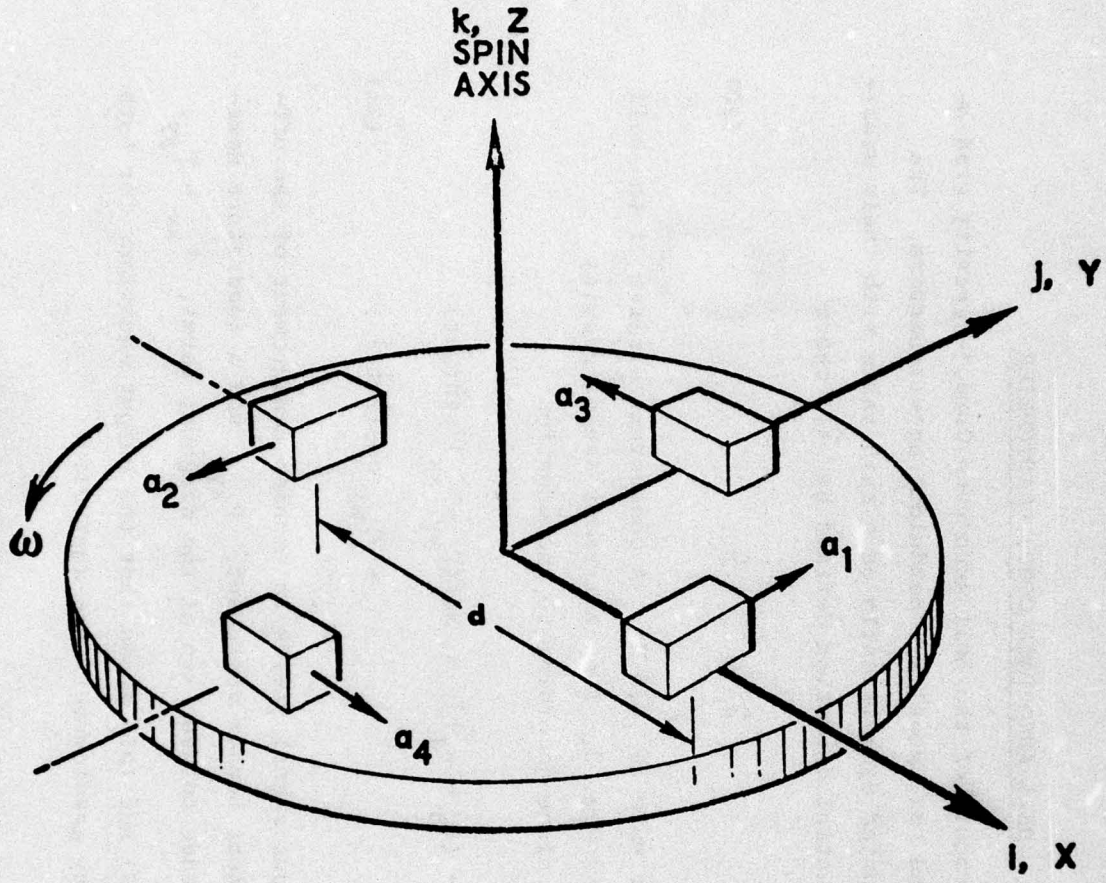

$$[(a_1 + a_2) - (a_3 + a_4)]_V = -2d(\Gamma_{xx} - \Gamma_{yy})\sin 2\omega t + 4d(\Gamma_{xy})\cos 2\omega t$$

FIG. 3 BELL AEROSPACE HEAVY PROOF MASS ACCELEROMETER GRADIOMETER

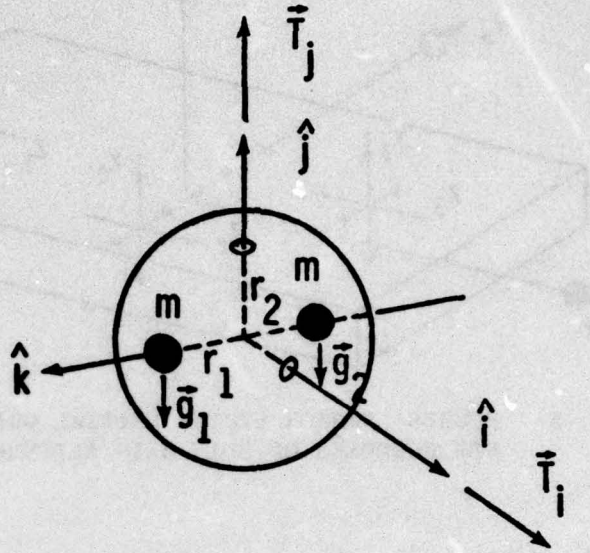

FIG. 4 SIMPLIFIED REPRESENTATION OF DRAPER LAB'S SPHERICAL GRAVITY GRADIOMETER; OUTPUT AXES $\hat{i}$ AND $\hat{j}$.

axis (k). The flotation fluid is inviscid, providing a degree of isolation from small amplitude (jitter) rotations of the case. The output vector equation for the spherical gradiometer is: [6]

$$[\vec{T}_g] = 2mr^2[-\Gamma_{yz}, \Gamma_{xz}, 0]^T \quad . \tag{22}$$

E. MEASURING THE GRAVITY GRADIENT WITH ROTATING GRAVITY GRADIOMETERS†

In Fig. 5, it is assumed that the sensors are not spinning and that and that the sensor axes (x_j, y_j, z_j) are respectively coincident with platform axes (x_p, y_p, z_p). The separate sensor reference system orientations can then be arbitrarily varied using a {1, 2, 3} Euler rotation

† Since the signal equations are the same for both the Hughes and Bell sensors, it is understood that the analysis of signal estimation for the Hughes' sensor applies directly to the Bell sensor also.

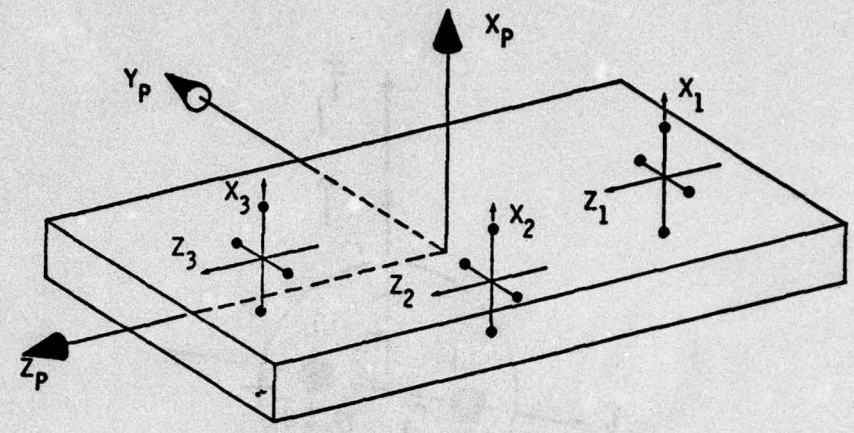

FIG. 5 HUGHES' SENSOR SYSTEM INITIAL ORIENTATION FOR PURPOSES OF SPIN AXIS ALIGNMENT SPECIFICATION

sequence defined by angles $\{\alpha_j, \beta_j, \gamma_j\}$. Subsequent to these alignment rotations, the sensors are spun up and measurements taken. The output of each sensor corresponds to (19), with each sensor measuring components of the gravity gradient tensor expressed relative to the newly specified body (sensor) reference directions. In order for these measurements to provide a complete estimate of the gravity gradient tensor, all six outputs from the three sensors must be related to a single reference frame. For convenience, this frame has been defined to be the platform reference frame. It is easy to show that

$$\vec{\vec{\Gamma}}_B = T_{B/P} \vec{\vec{\Gamma}}_P T_{B/P}^T \tag{23}$$

Sensor inphase and quadrature signals are averaged over a 10 sec sample period to provide measurements of $[\Gamma_{yy} - \Gamma_{xx}]_{Bj}$ and $[\Gamma_{xy}]_{Bj}$ as specified by (24) and (25),

$$[A_{IP}]_j = 4mr^2[\tfrac{1}{2}(\Gamma_{yy}-\Gamma_{xx})]_{Bj} \tag{24}$$

$$[A_Q]_j = 4mr^2[\Gamma_{xy}]_{Bj} \, . \tag{25}$$

Using (23), the right sides of (24) and (25) can be expressed in terms of the platform referenced gradient tensor for arbitrary Euler angle rotations $\{\alpha, \beta, \gamma\}_j$. Equations (24) and (25) can be rewritten for all three

sensors in terms of the platform referenced gradient tensor as

$$\frac{1}{4mr^2}\begin{bmatrix} A_{IP} \\ A_Q \end{bmatrix}_j = \left[\begin{array}{c|c|c|c|c|c} -\frac{1}{2}c^2_{\beta_j}c_{2\gamma_j} & \frac{1}{2}c_{2\gamma_j}\left(c^2_{\alpha_j}-s^2_{\alpha_j}s^2_{\beta_j}\right) & \frac{1}{2}c_{2\gamma_j}\left(s^2_{\alpha_j}-c^2_{\alpha_j}s^2_{\beta_j}\right) & -\frac{1}{2}c_{2\gamma_j}s_{2\beta_j}s_{\alpha_j} & \frac{1}{2}c_{2\gamma_j}s_{2\beta_j}c_{\alpha_j} & \frac{1}{2}c_{2\gamma_j}s_{2\alpha_j}\left(1+s^2_{\beta_j}\right) \\ & -\frac{1}{2}s_{2\gamma_j}s_{2\alpha_j}s_{\beta_j} & -\frac{1}{2}s_{2\gamma_j}s_{2\alpha_j}s_{\beta_j} & -\frac{1}{2}s_{2\gamma_j}c_{\beta_j}s_{\alpha_j} & -\frac{1}{2}s_{2\gamma_j}c_{\beta_j}s_{\alpha_j} & +c_{2\alpha_j}s_{2\gamma_j} \\ & \frac{1}{2}s_{2\gamma_j}\left(c^2_{\gamma_j}-s^2_{\beta_j}s^2_{\alpha_j}\right) & \frac{1}{2}s_{2\gamma_j}\left(s^2_{\gamma_j}-c^2_{\alpha_j}s^2_{\beta_j}\right) & c_{2\gamma_j}c_{\beta_j}c_{\alpha_j} & c_{2\gamma_j}c_{\beta_j}s_{\alpha_j} & \frac{1}{2}s_{2\gamma_j}s_{2\alpha_j}\left(1+s^2_{\beta_j}\right) \\ -\frac{1}{2}s_{2\gamma_j}c^2_{\beta_j} & +\frac{1}{2}c_{2\gamma_j}s_{\beta_j}s_{2\alpha_j} & -\frac{1}{2}c_{2\gamma_j}s_{2\alpha_j}s_{\beta_j} & -\frac{1}{2}s_{2\gamma_j}s_{2\beta_j}s_{\alpha_j} & +\frac{1}{2}s_{2\gamma_j}s_{2\beta_j}c_{\alpha_j} & +s_{\beta_j}\left(c_{2\gamma_j}s^2_{\alpha_j}-c_{2\alpha_j}c^2_{\gamma_j}\right) \end{array}\right] \begin{bmatrix} \Gamma_{xx} \\ \Gamma_{yy} \\ \Gamma_{zz} \\ \Gamma_{xy} \\ \Gamma_{xz} \\ \Gamma_{yz} \end{bmatrix}_{j=1,2,3} \tag{26}$$

$$\frac{1}{4mr^2}\left[A_j\right] = [M']\left[\vec{\Gamma}\right]. \tag{27}$$

The 6×6 matrix M' of (26) and (27) is singular due to the Laplace relationship of Γ_{xx}, Γ_{yy}, Γ_{zz} as shown in (5). The effect of this singularity can be removed either by eliminating one of the gradient tensor principal diagonal terms using (5) or by adding the Laplace equation to (26) as a 7th measurement having zero error. The addition of Laplace's equation as a measurement allows all of the terms of the gradient tensor to be treated in the same way mathematically. Combination of (5) with (27) yields

$$\frac{1}{4mr^2}\begin{bmatrix} A'_{6\times 1} \\ \hline 0 \end{bmatrix} = \begin{bmatrix} M'_{6\times 6} \\ \hline 1 \quad 1 \quad 1 \quad 0 \quad 0 \quad 0 \end{bmatrix} [\vec{\Gamma}] \tag{28}$$

or

$$[A] = [M]_{7\times 6}\, [\vec{\Gamma}] \, . \tag{29}$$

With

$$[B] \triangleq [M^T M]^{-1} [M^T] \tag{30}$$

the least squares error solution estimate of $[\vec{\Gamma}]$ is

$$[\hat{\Gamma}] = BA_M \tag{31}$$

where

$$A_M \triangleq A + V \, . \tag{32}$$

Matrix V is a 7×1 vector representing measurement noise. The first six terms of vector V are taken to be white, zero mean Gaussian random variables having variance $1\ (EU)^2$. The 7th component, V_7, is exactly zero. Furthermore,

$$\delta(V\ V^T) = \left[\begin{array}{c:c} I_{6\times 6} & 0_{7\times 1} \\ \hline 0_{1\times 6} & \end{array}\right] . \tag{33}$$

Equation (33) states that all six measurements have uncorrelated errors of variance $1\ EU^2$. With

$$\tilde{\vec{\Gamma}} \triangleq \hat{\vec{\Gamma}} - \vec{\Gamma} , \tag{34}$$

and

$$P_{6\times6} \triangleq \mathcal{E}[\tilde{\vec{\Gamma}}\ \tilde{\vec{\Gamma}}^T] , \tag{35}$$

$$P = B\ R\ B^T \tag{36}$$

where

$$R \triangleq \mathcal{E}[V\ V^T] . \tag{37}$$

Given (36), the problem is to find angles $(\alpha, \beta, \gamma)_j$ (which affect B) so that a scalar cost function J, which is related in some way to covariance matrix P is minimized. One reasonable specification for the cost function J is [cost function suggested by Prof. John V. Breakwell]

$$J \triangleq \mathrm{Tr}\{\mathcal{E}[\tilde{\tilde{\Gamma}}\ \tilde{\tilde{\Gamma}}^T]\} \tag{38}$$

where $\tilde{\tilde{\Gamma}}$ is defined by the 3x3 matrix composed of the errors in the estimate of $\vec{\Gamma}$. With $\tilde{\vec{\Gamma}}$ defined by (34),

$$\tilde{\tilde{\Gamma}} = \begin{bmatrix} \tilde{\Gamma}_1 & \tilde{\Gamma}_4 & \tilde{\Gamma}_5 \\ \tilde{\Gamma}_4 & \tilde{\Gamma}_2 & \tilde{\Gamma}_6 \\ \tilde{\Gamma}_5 & \tilde{\Gamma}_6 & \tilde{\Gamma}_3 \end{bmatrix} \tag{39}$$

and

$$\mathcal{E}[\tilde{\tilde{\Gamma}}\tilde{\tilde{\Gamma}}^T] = \mathcal{E}\begin{bmatrix} \tilde{\Gamma}_1^2+\tilde{\Gamma}_4^2+\tilde{\Gamma}_5^2 & \tilde{\Gamma}_1\tilde{\Gamma}_4+\tilde{\Gamma}_4\tilde{\Gamma}_1+\tilde{\Gamma}_5\tilde{\Gamma}_6 & \tilde{\Gamma}_1\tilde{\Gamma}_5+\tilde{\Gamma}_4\tilde{\Gamma}_6+\tilde{\Gamma}_5\tilde{\Gamma}_3 \\ & \tilde{\Gamma}_4^2+\tilde{\Gamma}_2^2+\tilde{\Gamma}_6^2 & \tilde{\Gamma}_4\tilde{\Gamma}_5+\tilde{\Gamma}_2\tilde{\Gamma}_6+\tilde{\Gamma}_6\tilde{\Gamma}_3 \\ & & \tilde{\Gamma}_5^2+\tilde{\Gamma}_6^2+\tilde{\Gamma}_3^2 \end{bmatrix} \tag{40}$$

The off-diagonal terms of (40) are all zero, and

$$\mathrm{Tr}\ \mathfrak{S}[\tilde{\tilde{\Gamma}}\tilde{\tilde{\Gamma}}^T] = \sum_{i=1}^{3} \tilde{\Gamma}_i^2 + 2 \sum_{i=4}^{6} \tilde{\Gamma}_i^2 \ . \tag{41}$$

With

$T \triangleq$ orthonormal transformation matrix relating the expression of a vector in reference system A to its expression in reference system B,

and since

$$\vec{\vec{\Gamma}}_A = T \vec{\vec{\Gamma}}_B T^T \ . \tag{42}$$

Using (42) it is easy to show that

$$\tilde{\tilde{\Gamma}}_A = T \tilde{\tilde{\Gamma}}_B T^T \ . \tag{43}$$

Hence,

$$\tilde{\tilde{\Gamma}}_A \tilde{\tilde{\Gamma}}_A^T = T \tilde{\tilde{\Gamma}}_B T^T T \tilde{\tilde{\Gamma}}^T T^T \tag{44}$$

and since the trace is invariant under similarity transformation,

$$\mathrm{Tr}\{\mathfrak{S}[\tilde{\tilde{\Gamma}}_A \tilde{\tilde{\Gamma}}_A^T]\} = \mathrm{Tr}\{\mathfrak{S}[\tilde{\tilde{\Gamma}}_B \tilde{\tilde{\Gamma}}_B^T]\} \ . \tag{45}$$

Therefore the cost function J defined by (38) is invariant under linear transformation. This invariance allows the cost function to provide a scalar measure of the quality of the gradient estimate without regard for the coordinate system to which the measurements are referenced.

The system shown in Fig. 6 is taken as the baseline gradient measurement case. The spin axis of each sensor is parallel to a different platform reference direction. For this sensor system orientation, J had the value $8.667\ EU^2$. The Euler angles corresponding to this set of sensor orientations are listed in (46),

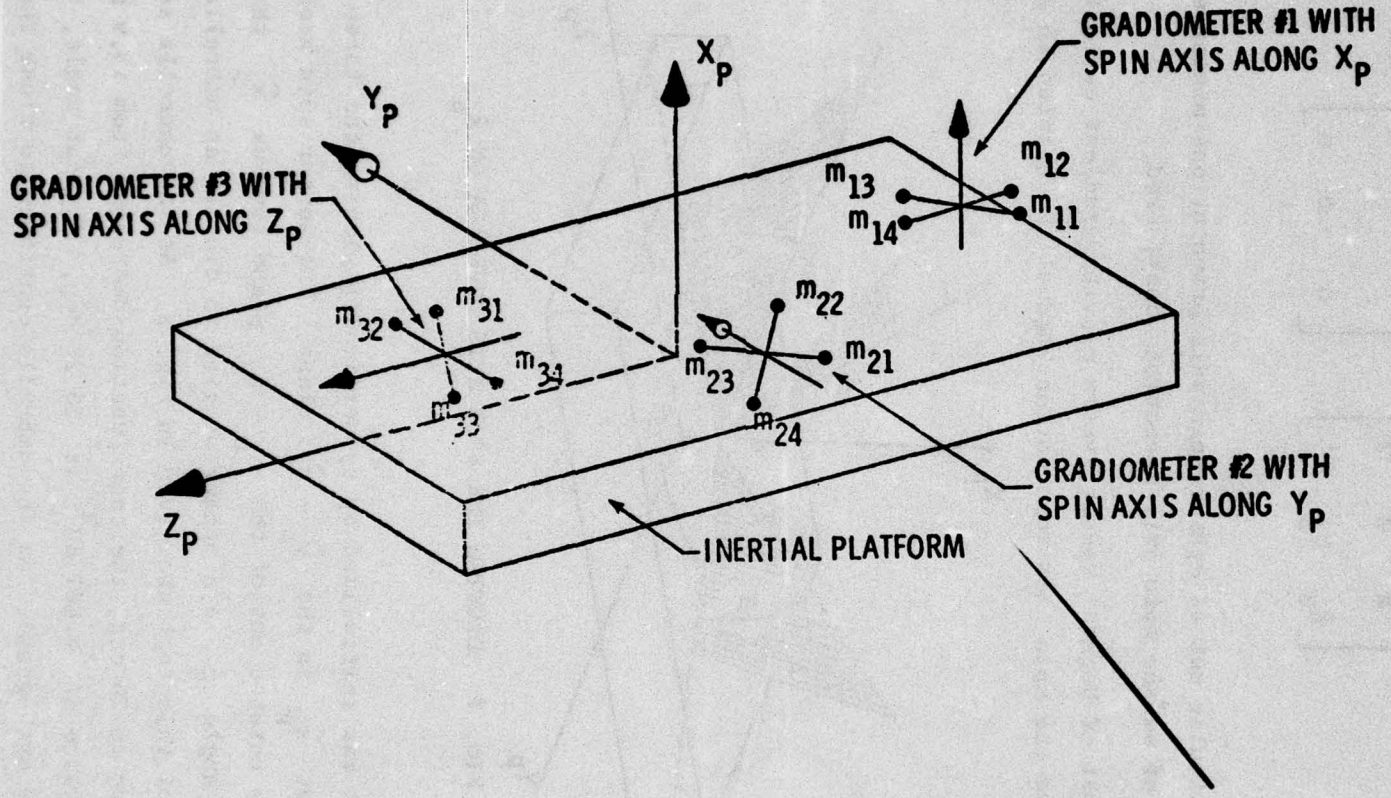

FIG. 6 BASELINE HUGHES' GRADIOMETER GRADIENT MEASURING SYSTEM

$$\begin{bmatrix} \alpha_1 & \beta_1 & \gamma_1 \\ \alpha_2 & \beta_2 & \gamma_2 \\ \beta_3 & \beta_3 & \gamma_3 \end{bmatrix} = \begin{bmatrix} 0 & 90 & 0 \\ 270 & 0 & 0 \\ 0 & 0 & 0 \end{bmatrix} \text{ deg} \qquad (46)$$

This particular set of sensor spin axis orientations minimized J for all sets of sensor spin axis directions considered.

A test of Hughes' sensor system gravity gradient estimation for the case where the spin axes were not orthogonal is depicted in Fig. 7.

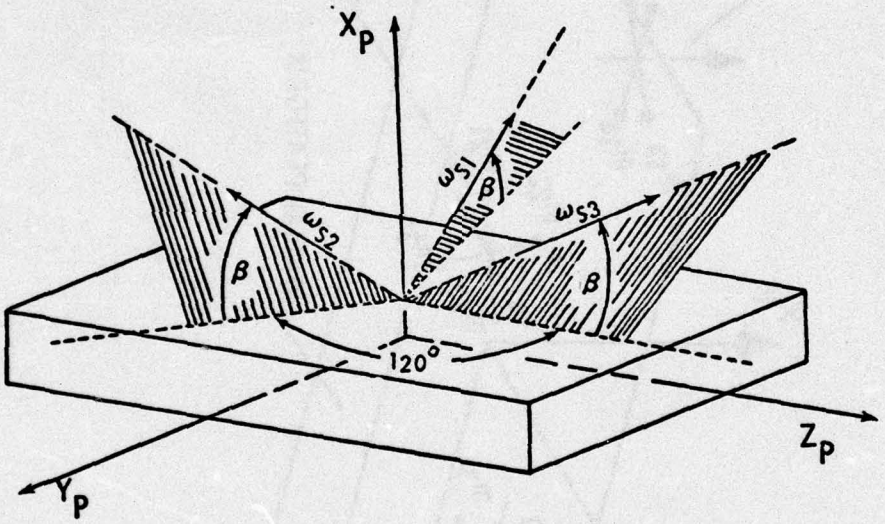

FIG. 7 CLOSING THE SPIN AXIS UMBRELLA ON $\hat{x}_p$

This test was initialized by symmetrically placing the three sensor spin axes about $\hat{x}_p$ in the $\hat{y}_p - \hat{z}_p$ plane. The sensor spin axes were then uniformly rotated out of the $\hat{y}_p - \hat{z}_p$ plane towards $\hat{x}_p$ through an increasing angle β in a manner similar to closing an umbrella. The results of this test are given in Fig. 8. As the umbrella angle increased from 5 deg to 35 deg, the cost function decreased from 13.9 EU^2 to its minimum value of 8.667 EU^2 at 35.26 deg. At that angle, the spin axes were orthogonal. As the umbrella continued to close, the cost function again began to increase, principally due to a loss in the accuracy of the Γ_{xx} estimate.

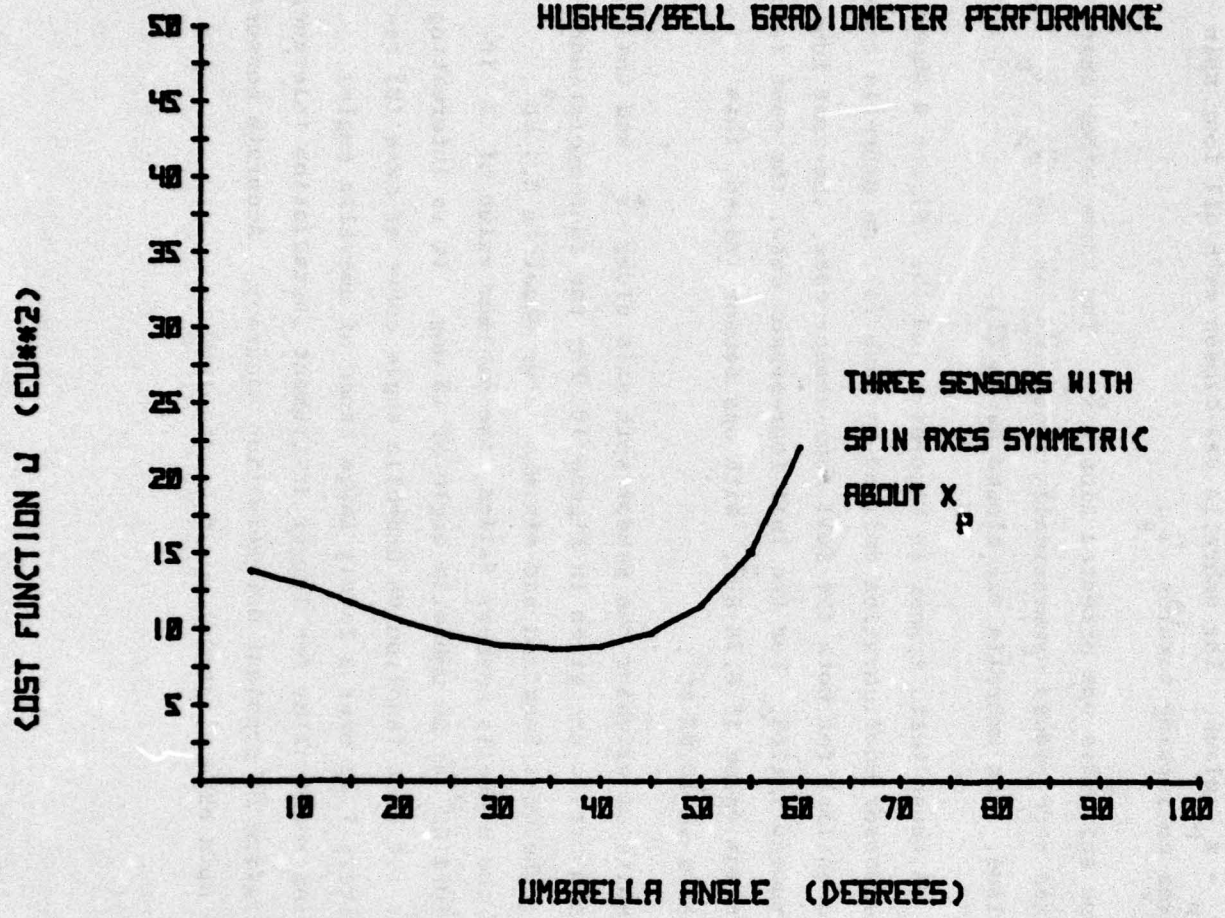

FIG. 8 HUGHES' SENSOR SYSTEM GRADIENT ESTIMATE ERROR COST FUNCTION AS UMBRELLA ANGLE INCREASES FROM ZERO TO 60 DEGREES.

The cost function analysis was extended to the 4-instrument case. A fourth instrument provides protection against loss of mission due to the failure of a single gradiometer. Several four-instrument operating configurations were considered. These were:

(1) All four spin axes were symmetrically placed about $\hat{x}_p$ in the $\hat{y}_p - \hat{z}_p$ plane. The umbrella was closed with all four spin axes collapsing towards $\hat{x}_p$;

(2) One spin axis was oriented along $\hat{x}_p$. The three other spin axes were placed symmetrically about $\hat{x}_p$ in the $\hat{y}_p - \hat{z}_p$ plane. The umbrella was closed as in (1).

The results of these tests appear in Figures 9 and 10. Figure 9 shows that for the sensor configuration defined by case (1), an umbrella angle of 35 deg is optimal for both the full four-sensor case, the cost func- of one instrument failed. For the full four-sensor case, the cost function has minimum value of 6.38 EU^2. With one sensor failed, this value increased to 10.63 EU^2.

The results of aligning one sensor spin axis along $\hat{x}_p$ and the three others in an umbrella are given in Figure 10. For the four-operational sensor case, the cost function had minimum value equal to 6.4 EU^2. With one of the umbrella sensors failed, the minimum value of J increased to 10.4 EU^2 at an umbrella angle of 15 deg. It is interesting to note that the cost function vs umbrella angle curve of case (2) remains relatively flat over a fairly large range of umbrella angles. This situation would allow for larger instrument installation tolerances without sacrifice of gradient determination accuracy. Accurate measurement of the spin axis alignment would be required.

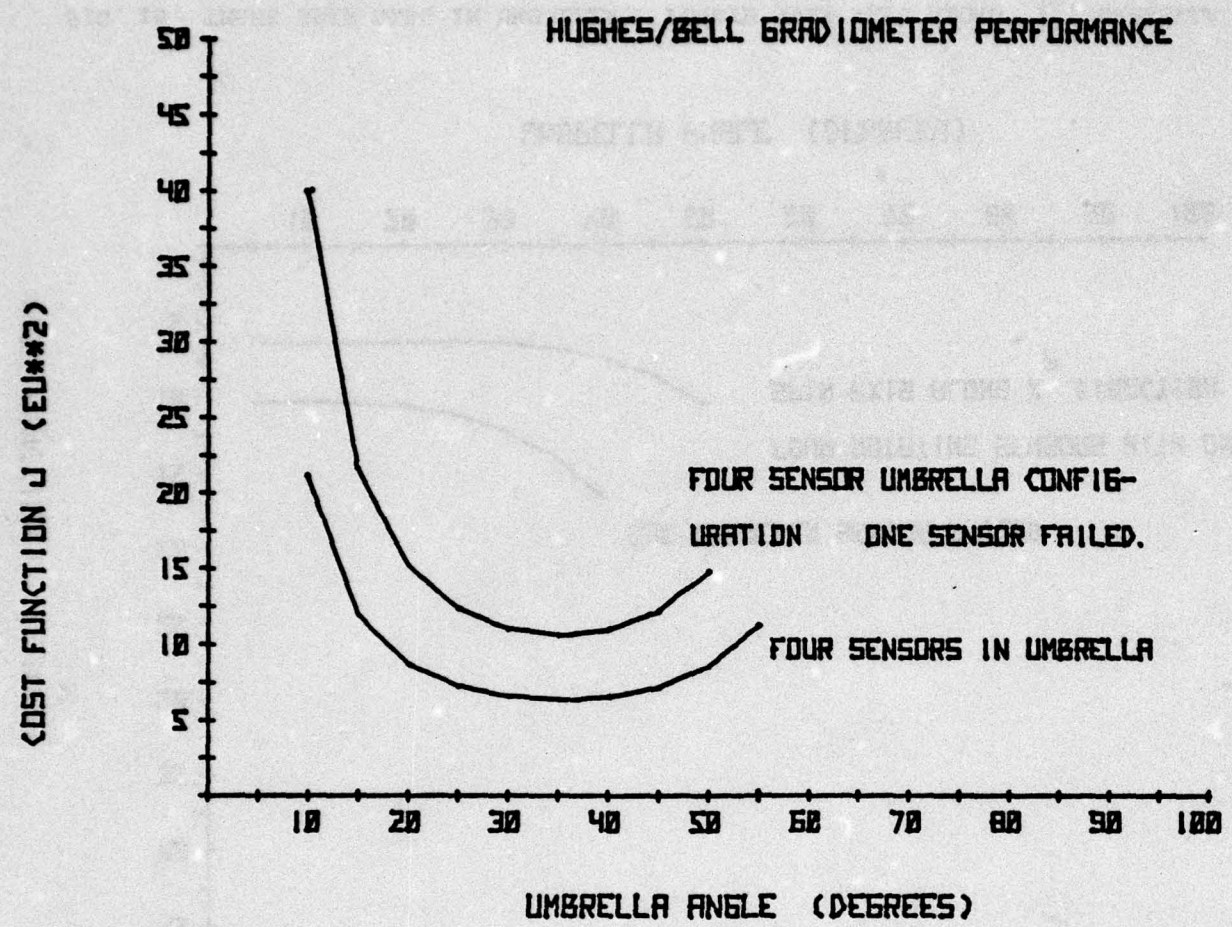

FIG. 9 ALL FOUR SPIN AXES IN THE UMBRELLA, SYMMETRIC SPIN AXIS PLACEMENT (90 deg intervals) ABOUT $\hat{x}_p$.

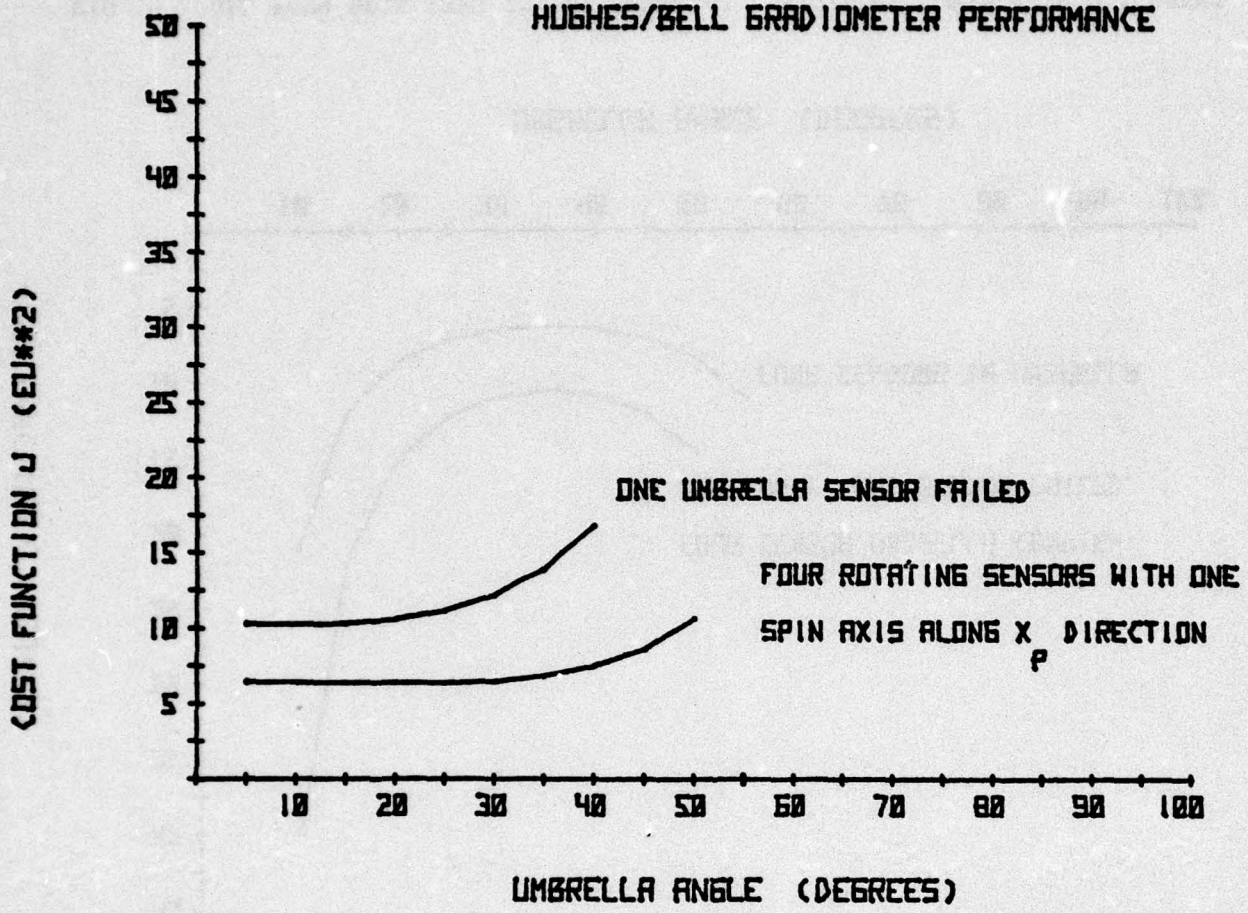

FIG. 10 THREE SPIN AXES IN UMBRELLA. FOURTH SPIN AXIS ALONG $\hat{x}_p$. UMBRELLA SENSOR SPIN AXES SYMMETRICALLY PLACED ABOUT $\hat{x}_p$ (120 deg intervals).

F. MEASURING THE GRAVITY GRADIENT TENSOR WITH THE DRAPER LAB GRAVITY GRADIOMETER

An orientation analysis similar to that carried out for the rotating gradiometers was also carried out for the Draper Lab's static instrument system. For a gradiometer triad composed of three spherical sensors, the defining equation has the form of (47). Matrix M of (47) is similar in nature to M' of (28) in that it is composed of products of Euler rotations. Note that the scalar multiplicative coefficient for this instrument is $2mr^2$, whereas it was $4mr^2$ for the Hughes' sensor.

$$\begin{bmatrix} A_{1\hat{i}} \\ A_{1\hat{j}} \\ A_{2\hat{i}} \\ A_{2\hat{j}} \\ A_{3\hat{i}} \\ A_{3\hat{j}} \\ 0 \end{bmatrix} = 2mr^2 \left[\begin{array}{c} M_{6\times 6} \\ \hline 1\ 1\ 1\ 0\ 0\ 0 \end{array}\right] \begin{bmatrix} \Gamma_{xx} \\ \Gamma_{yy} \\ \Gamma_{zz} \\ \Gamma_{xy} \\ \Gamma_{xz} \\ \Gamma_{yz} \\ \end{bmatrix} \qquad (47)$$

The analytical development of the gradient tensor estimate for this instrument system is similar to that of the Hughes' instrument and appears in Ref. 6. Optimal sensor orientation is again defined to be that which minimizes the cost function specified in (38). The results of the three-instrument analysis are shown in Fig. 11. For the Draper Lab's sensor, the between-the-weights axis has essentially the same significance as the spin axis has for the rotating sensors. The $\hat{j}$ axis angular rotations, β, are identical to the umbrella angles discussed in connection with the Hughes' sensor spin axis orientations.

The performance plots of Fig. 11 show that the cost function J is minimized when the between-the-weights axes are symmetrically located about $\hat{x}_p$ and rotated out of the $\hat{y}_p - \hat{z}_p$ plane through an umbrella angle of approximately 58 degrees. The value of J at that point was found to be approximately 10.8 EU^2. Note that for the symmetric between-the-weights axes case, a singularity exists at an umbrella angle of 35.2644 deg. It is easy to show that a singularity always exists for this three sensor system when the between-the-weights axes form an orthogonal triad [6].

Four sensor gradient tensor estimation was also considered for the Draper Lab's sensor. The following cases were considered:

(1) Four sensors symmetrically located about $\hat{x}_p$ having identical umbrella angles β;

(2) A single sensor having its between-the-weights axis vertical. Three sensors symmetrically located about $\hat{x}_p$ having identical umbrella angles β.

The results of these tests for the four-sensor and one-sensor-failed cases are given in Figs. 12 and 13.

The cost function vs umbrella angle curve for the case where all four between-the-weights (BTW) axes are symmetrically spaced about $\hat{x}_p$ appears in Fig. 12. With four sensors operating, the minimum cost function occurred at an umbrella angle of 50 deg and had a value of 7.1 EU^2. With one sensor failed, the minimum value of the cost function increased to 11.9 EU^2 at 55 deg.

The effect of removing one of the BTW axes from the umbrella and placing it along $\hat{x}_p$ is shown in Fig. 13. For this case, the minimum value of J occurs at an umbrella angle of 20 deg and has value equal to 8.25 EU^2. At β equal to 55 deg, the value of J is 8.6 EU^2. With one umbrella sensor failed, the minimum value of the cost function was found to be 12.66 EU^2 at an umbrella angle of 35 degrees.

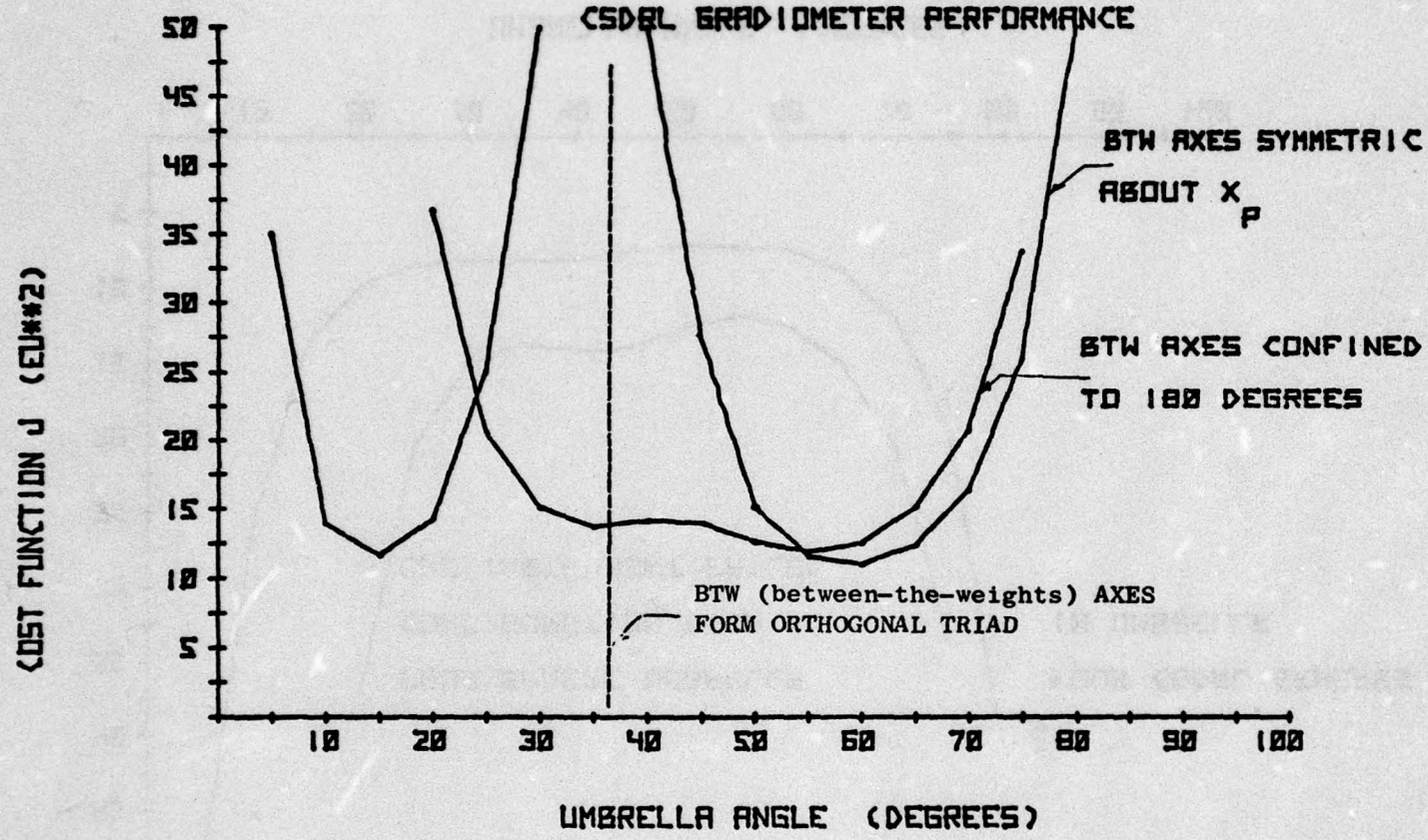

FIG. 11 GRADIENT MEASUREMENT USING THREE DRAPER LAB GRADIOMETERS

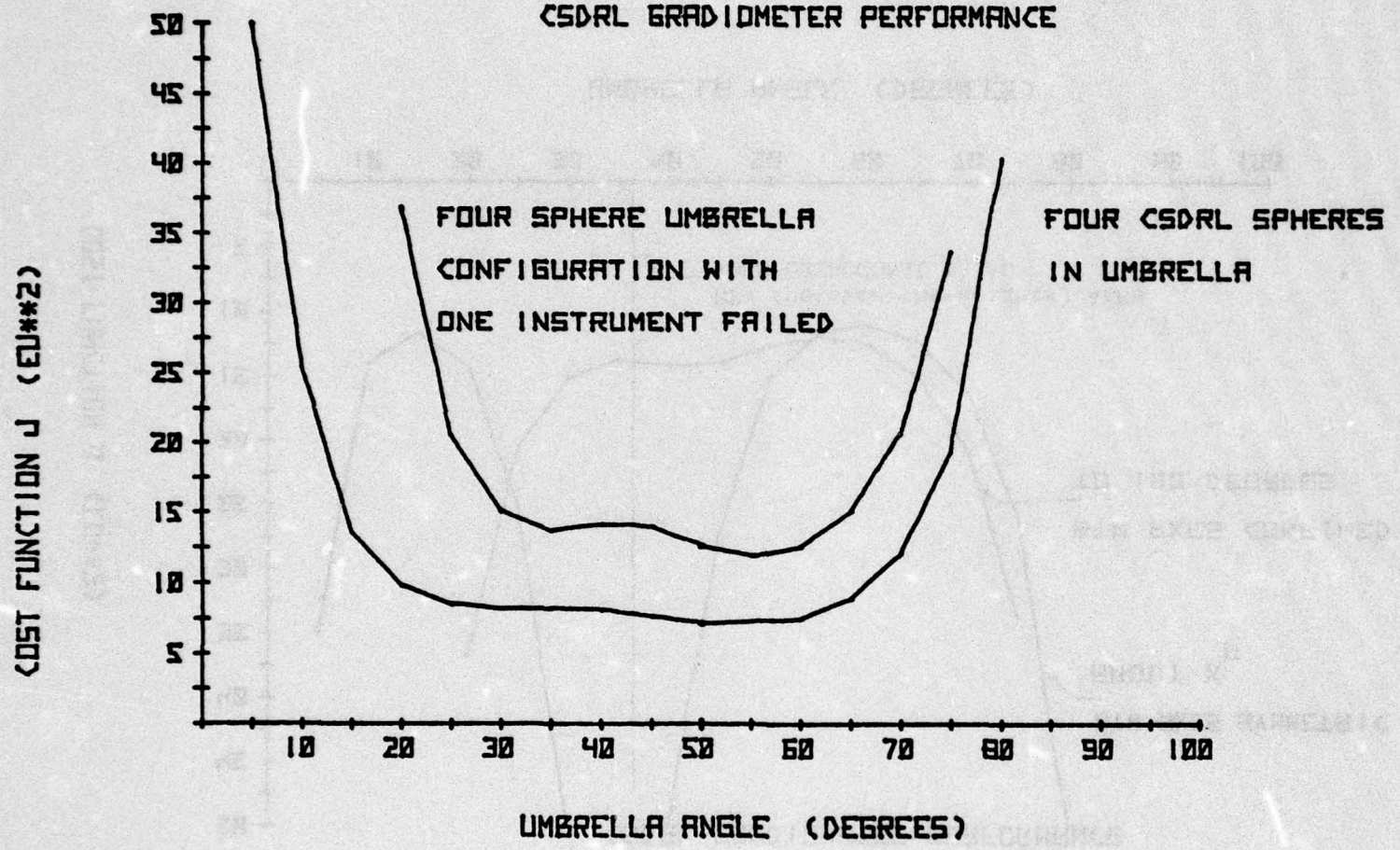

FIG. 12 GRADIENT ESTIMATION WITH FOUR DRAPER LAB'S (CSDRL) SPHERICAL SENSORS. ALL FOUR BTW (between-the-weights) AXES LIE IN THE UMBRELLA.

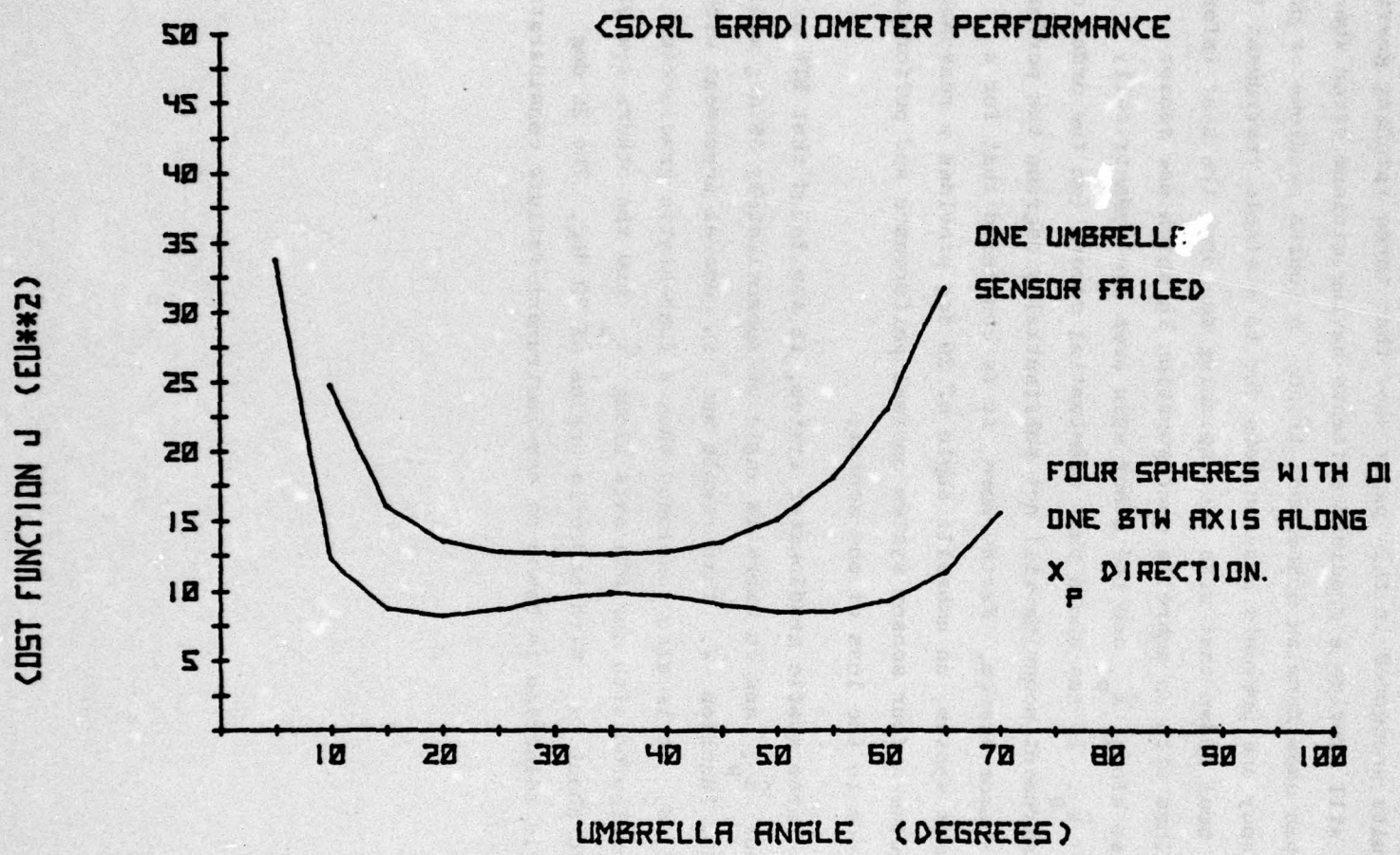

FIG. 13 GRADIENT ESTIMATION WITH FOUR CSDRL SPHERICAL SENSORS. ONE BTW AXIS LIES ALONG $\hat{x}_p$. OTHER BTW AXES SYMMETRICALLY SPACED ABOUT $\hat{x}_p$.

G. CONCLUSIONS

The results presented in this paper show that three spinning gravity gradiometers will provide a gradient estimate having minimum error when the sensor spin axes form an orthogonal triad. A fourth gradiometer provides redundancy and prevents mission loss due to a single instrument failure. It has been shown that with four spinning sensors, the best information is obtained with an umbrella configuration in which one sensor spin axis lies along $\hat{x}_p$, and the other spin axes are symmetrically spaced about $\hat{x}_p$. It was shown that substantial errors (on the order of 5 deg) in instrument mounting will not substantially degrade the performance of the sensor system. Furthermore, it is concluded that for a spinning sensor system, an umbrella angle of 20 deg provides a reasonable compromise between four sensor system optimal performance and performance degradation due to the loss of one sensor.

For the three static gradiometer system, it was found that BTW axis symmetry about $\hat{x}_p$, and an umbrella angle of approximately 58 deg minimized the cost function J. This result was in general agreement with those of Ref. 4. It is also concluded that a four-static gradiometer system be configured with one BTW axis along $\hat{x}_p$ and the others symmetrically located about x_p with umbrella angles of 20 deg. The 20 deg umbrella angle selection is based on one-instrument-failure considerations.

Chapter II

STRESS RELAXATION

The phenomena of creep, creep recovery, relaxation, microstrain, or whatever term is applied, are described in a variety of ways, the reason for which is apparent disagreement of the actual mechanism involved. Johnson [7] considers metal as an aggregate of crystalline domains embedded in a viscous medium (the intercrystalline boundary). Assuming, for the moment, three stages of creep, the first stage is postulated to occur by viscous motion of the intercrystalline boundary. The second stage occurs by slipping of the crystalline domains within the boundary, and the third stage by fragmentation of the crystalline domains.

As material grain size increases, creep rate decreases due to the reduction in the number of intercrystalline boundaries. The extension of this, of course, is that single crystals would exhibit no viscous creep.

Orowan [8] claims single crystals do creep due to slip of atoms within the crystalline lattice. He further asserts that the stress at which a single crystal begins to yield depends on the amount of prior strain, i.e., the strain history.

Creep is commonly described as occuring in three stages:

(1) The primary stage during which strain decreases rapidly with time;

(2) The secondary stage when the strain rate remains fairly constant;

(3) The tertiary stage in which strain increases rapidly.

During the primary stage, the creep rate decreases rapidly due to a buildup in crystal dislocations which pile up and inhibit the viscous flow.

The secondary stage is a tug-of-war between strain hardening and reduction in specimen cross section resulting in an essentially constant strain rate [9].

Lubahn and Felgar [10] argue that creep should not always be described in terms of these three stages but rather that creep curves can be conveniently described thusly. For a metallurgically stable metal subjected to constant stress, creep will always be of a primary nature. If the load is held constant, there will be a tendency for the creep rate to increase.

One exception to the generalization of diminishing creep rate was reported by Chalmers [11]. In room temperature tests of tin crystals at low stresses ($\sim$ 200 psi) the creep rate was constant for a time and then decreased to a small value. This value was about half the initial rate. It was also observed that the initial rate was proportional to stress giving rise to a conclusion that the action was viscous at low stresses and strains. At higher stresses and strains, the behavior was more typical of a metallurgically stable metal. Chalmers termed this behavior 'microplasticity'. Theories which explain creep in terms of viscous phenomena are termed 'phenomenological' since the concept of a viscosity coefficient is a phenomenological entity [12], [13].

The two principal mechanisms by which creep of single crystals occurs are termed 'slip' and 'grain rotation'. Slip refers to shearing displacement of parts of the same crystal. The plane on which slip occurs is the slip band. Grain rotation is, as you might suspect, angular displacement relative to neighboring grains [10]. As slip continues to occur, the number of areas where this happens (dislocations) increases and eventually opposes the slipping action. This is the mechanism of strain hardening [Refs. 7, 14, 15, 16, and 17].

A material which elongates when first loaded, continues to stretch under constant load and recovers less than all the elongation upon removal of the load behaves, in part, like a viscous liquid and partly like an elastic solid; hence, the description viscoelastic material.

If one accepts the phenomenological theories, all metallurgically stable metals could be termed viscoelastic. Usually, however, the term is applied to materials such as plastics, solid fuel propellants, rubber, and glass.

For analysis purposes, materials that creep are represented as one of three models:

Maxwell model is represented by a linear spring and linear dashpot connected in series. When loaded, such a material responds with instantaneous elastic strain followed by continuously creeping strain. Unloading results in only partial recovery of strain.

Kelvin model is represented by a linear spring and linear dashpot connected in parallel. A Kelvin material, when loaded, first begins to creep at a rate that decreases to zero. Unloading results in gradual recovery to the original size.

Three element or Burgers model is simply a Maxwell and a Kelvin model connected-on series. This type material displays instantaneous elastic response, creep with time, elastic memory; and permanent deformation under load. Removal of the load results in partial strain recovery.

Creep recovery is most easily explained in terms of viscous behavior. For most polycrystalline metals, the amount of creep recovery is very small, whereas in plastics, it is more pronounced.

The time required for the load, when held at constant strain, to relax to 1/e of its original value is termed the 'relaxation' time [18], [19]. Thus a viscoelastic material is characterized by moduli that are time dependent and type-of-loading dependent. Since most viscoelastic materials behave linearly over some range, it is possible to identify those limits in terms of stress, strain, and time, and the stress-strain-time behavior of the material can be fairly accurately predicted for design purposes [20].

Materials for use in gravity gradiometer design, regardless of what they are, will exhibit some degree of creep, creep recovery, or stress relaxation and this effect must be taken into account [21].

REFERENCES

1. Ames, C.B., R.L. Forward, et. al., "Prototype Moving Base Gravity Gradiometer;" R&D Design Evaluation Rept, Hughes Research Labs, Malibu, Calif., Jan 1973.

2. Metzger, E.H., and A. Jircitano, "Analysis of Real Time Mapping of Horizontal and Vertical Gravity Anomalies Aboard A Moving Vehicle Such as an Aircraft," Int'l Symposium on Application of Marine Geodesy, Columbus, Ohio, Jun 1974.

3. Trageser, M.B., "A Gradiometer System for Gravity Anomaly Surveying," from Advances in Dynamic Gravimetry, Proc. of the Symposium on Dynamic Gravimetry, (T. Kattner, editor), Fort Worth, Texas, Mar 1970.

4. Trageser, M.B., "Feasibility Model Gravity Gradiometer Test Results", AIAA Guidance & Control Conf., Boston, Mass, Aug 1975, paper No. 75-1093.

5. Karamcheti, K., Vector Analysis and Cartesian Tensors, Holden-Day, Inc., San Francisco, Calif., 1967.

6. DeBra, D.B., and E.J. Pelka, "Gravity Gradiometer Signal Detection, Parameter Identification, and Online Parameter Control," AFGL Final Report., Contract F 19628-76-C-0109, to be published.

7. Jahsman, W.E., "A Survey of Phenomenological Creep Laws for Metallurgically Stable Polycrystalline Metals at Constant Temperature," Lockheed Missiles and Space Co., Sunnyvale, Ca., Rept. No. LMSD-2411, May 1958.

8. Orowan, E., "Creep in Metallic and Nonmetallic Materials," Proc. of the 1st U.S. National Congress of Applied Mechanics, ASME 1952, p. 453.

9. Freudenthal, A.M., The Inelastic Behavior of Engineering Materials and Structures, Wiley, 1950.

10. Lubahn, J.D., and Felgar, Plasticity and Creep of Metals, Wiley, 1961.

11. Chalmers, B., "Microplasticity in Crystals of Tin," Proc. of Royal Society (London) 156A, 1936.

12. Hult, J.A.H., Creep in Engineering Structures, Blaisdell Pub., 1966.

13. Shimmin, K.D., "Applicability of Present Creep Prediction Techniques for Extrapolating Very-Long Time Creep Behavior," Wright Air Dev, Div. WADD TR-60-523.

14. Gilman, J.J., Problems of Plasticity, Leiden Noordkoff Int. Publ., p. 177-191, 1974.

15. Krempl, E., Acta Mechanica, Vol. 22, No. 1-2, pp. 53-90, 1975.

16. McCartney, L.N., and McLean, "Strain/Time Relations Describing Creep," J. of Mech Eng Science, Vol. 18, pp. 39-45, Feb. 1976.

17. Besseling, J.F., "A Theory of Small Deformations of Solid Bodies," AFOSR-TN-59-605.

18. Hall, I.H., Deformation of Solids, London - Nelson, 1968.

19. Alexander, R.L., "Materials That Creep," Machine Design, pp. 120-127, Mar 3, 1966.

20. DeBatert, R., Stress Relaxation, A Review of Principles and Applications Reviews on the Deformation Behavior of Materials, Vol. I, No. 2, 1975.

21. Krasovikii, A.A., "The Critical Sensitivity of Instruments with Large Relaxation Times — Gravity Gradiometers, (Russian) Akademiia Nauk SSSR, Doklady, Vol. 2231, July 1975, pp. 83-86.

☆U.S. GOVERNMENT PRINTING OFFICE: 1977-A-0638/93